CrystEngComm

PAPER

View Article Online
View Journal | View Issue

Cite this: *CrystEngComm*, 2014, **16**, 9216

Fabrication and photoluminescence properties of TiO_2:Eu^{3+} microspheres with tunable structure from solid to core–shell

Ming Yan,[b] Haifeng Zou,[a] Huan Zhao,[a] Yanhua Song,[a] Keyan Zheng,[a] Ye Sheng,*[a] Guanjun Wang*[b] and Qisheng Huo[c]

Received 21st May 2014,
Accepted 12th August 2014

DOI: 10.1039/c4ce01048e

www.rsc.org/crystengcomm

Monodisperse solid and core–shell structured TiO_2:Eu^{3+} microspheres have been successfully prepared by a facile one-step hydrothermal method using polyethylene glycol (PEG, MW 20 000) as the soft template, titanium tetrabutoxide (TBOT) as the titanium source, and ethanol as the solvent. The XRD patterns show that the direct hydrothermal synthesized products are anatase titanium dioxides. TEM and SEM observations indicate that the amount of ethanol plays an important role in the formation of TiO_2:Eu^{3+} microspheres. Solid TiO_2:Eu^{3+} microspheres are formed by using small amounts of ethanol, while core–shell structured ones are formed by using large amounts of ethanol. Possible growth mechanisms of both the solid and the core–shell structured TiO_2:Eu^{3+} microspheres are also proposed in this paper. In addition, without any further calcination, the direct hydrothermal synthesized solid and core–shell structured TiO_2:Eu^{3+} microspheres show strong red emission corresponding to the $^5D_0 \rightarrow {}^7F_2$ transition of the Eu^{3+} ions under ultraviolet excitation. However, the luminescence intensity of the solid microspheres is much higher than that of the core–shell structured TiO_2:Eu^{3+} microspheres, which might be due to the fewer defects and much more effective doping of Eu^{3+} ions into the solid microspheres.

1. Introduction

In recent years, fabrication of three-dimensional (3D) microspheres including solid and core–shell structures has attracted considerable attention due to their excellent properties and potential applications.[1–3] Thus, great efforts have been dedicated to explore new approaches for the fabrication of microspheres in different systems. Among various synthesis methods, the hydro/solvothermal process has been proved to be one of the most effective and convenient synthesis techniques in obtaining microspheres owing to its mild reaction conditions, tunable reaction parameters, and large-scale production capability.[4–6] However, it's well known that the reaction parameters, such as reaction time and temperature, pH value of the precursor solution, and surfactants and solvents used, affect the crystal growth behavior directly.[7,8] Therefore, it is important to clarify the effect of reaction conditions on the sample shape and discuss the formation mechanisms of different morphologies which will guide the design and preparation of new inorganic functional materials.[9]

Due to its chemical stability, easy synthesis, low cost, non-toxicity, and non-hygroscopic performance, titania (TiO_2) is suggested to be a promising host material for the luminescence of various rare earth ions.[10–12] Therefore, many efforts have been devoted to explore various morphologies of TiO_2-based phosphors, such as nanorods,[13] nanotubes,[14] nanowires,[15] nanorings,[16] nanoplates,[17] microspheres,[18,19] core–shell structures,[20] hollow spheres,[21] *etc.* However, to the best of our knowledge, there have been few reports on the synthesis and the corresponding luminescence of uniform, well-dispersed submicron-scale Eu-doped TiO_2 spheres with tunable structure from solid to core–shell.

The synthesis of core–shell structured TiO_2 microspheres *via* the Ostwald ripening process reported by Yuming Cui *et al.*,[22] Zeng's group,[23] and Hexing Li *et al.*[24] has attracted significant scientific interest. The interest is motivated by their adjustable morphology, size, and interior structure. However, in these reports, the effect of the amount of solvent on the morphology of the products hasn't been mentioned. This work, for the first time, reports the synthesis of TiO_2:Eu^{3+} spheres with tunable structure from solid to core–shell by simply tuning the amount of ethanol. The possible formation mechanisms are suggested. In addition, the shell and core sizes of the core–shell structured TiO_2:Eu^{3+} microspheres can also be easily tuned by controlling the hydrothermal time through the Ostwald ripening process.

[a] *College of Chemistry, Jilin University, Changchun 130012, PR China. E-mail: shengye@jlu.edu.cn*
[b] *Spine Center of the First Hospital of Jilin University, Changchun 130021, PR China*
[c] *State Key Laboratory of Inorganic Synthesis and Preparative Chemistry, College of Chemistry, Jilin University, Changchun 130012, PR China*

Without any further calcination, the direct hydrothermal synthesized solid and core–shell structured spheres show strong red emission under ultraviolet excitation, but their luminescence intensities are different. The possible reason is discussed.

2. Experimental section

2.1. Materials

$Eu(NO_3)_3$ aqueous solution was obtained by dissolving Eu_2O_3 (99.99%) in dilute HNO_3 solution under heating with agitation. All other chemical reagents were of analytical grade and used without further purification.

2.2. Synthesis

In a typical experimental procedure, 2.0 g of PEG was dissolved in 18 mL of ethanol under heating. After the solution was cooled to room temperature, 1.2 mL of HCl, 2.4 mL of glacial acetic acid, and a specific amount of $Eu(NO_3)_3$ were added and stirred for 5 min. 1.7 mL of tetrabutyl titanate was dropped into the above mixture solution and then 1.0 g of urea ($CO(NH_2)_2$) was added and stirred again for 10 min. Finally, the mixture was transferred into a Teflon-lined stainless steel autoclave (50 mL capacity). The autoclave was heated and maintained at 180 °C for 12 h and then allowed to cool to ambient temperature naturally. After the reaction, the products of the hydrothermal reaction were collected, washed with distilled water and ethanol four times alternately, and dried in air for 12 h at 60 °C. The resulting sample was labeled as S1. When the amount of ethanol added was 30 mL, holding the other conditions constant, the resulting sample was labeled S2. Parallel experiments were carried out to examine various synthetic parameters.

2.3. Characterization

X-ray diffraction (XRD) experiments were carried out using an XRD-6000 X-ray diffractometer (Shimadzu) with Cu Kα radiation (λ = 0.154056 nm). The size and morphology of the samples were inspected using a field emission scanning electron microscope equipped with an energy-dispersive spectrometer (EDS) (FE-SEM, S-4800, Hitachi, Japan). The transmission electron microscopy (TEM) images were obtained using a FEI Tecnai G^2 S-Twin transmission electron microscope with a field emission gun operating at 200 kV. The photoluminescence spectra (PL) were observed using a Jobin Yvon FluoroMax-4 equipped with a 150 W xenon lamp as the excitation source. All of the measurements were performed at room temperature. The X-ray photoelectron spectra (XPS) were taken using a VG ESCALAB 250 electron energy spectrometer with Mg Kα (1253.6 eV) as the X-ray excitation source.

3. Results and discussion

Fig. 1(A) shows the X-ray diffraction (XRD) patterns of TiO_2:Eu^{3+} solid microspheres (S1) and core–shell microspheres (S2) which indicate that both S1 and S2 are all anatase phases of titania. The strong and sharp diffraction peaks indicate the good crystallinity of the as-synthesized products obtained by the direct hydrothermal process without further sintering. The anatase phase with good crystallinity is beneficial to the luminescence of Eu^{3+} ions.[25] Careful observation shows that the positions of XRD peaks, especially the prominent (101) peaks of S1 and S2, are shifted toward much higher 2θ values compared with that of the standard XRD pattern, as shown in Fig. 1(B). This is attributed to the large mismatch in the ionic radius between Eu^{3+} and Ti^{4+}. For hetero-valence ion doping, the variations of the crystal lattice are complex due to the requirement of extra vacancy or interstitial ions to compensate charge.[26] Therefore, we can't infer the position of Eu^{3+} doping, but the notable angle shifts of S1 and S2 compared with the standard XRD pattern indicate that Eu^{3+} ions have been doped into the TiO_2 crystal lattice. In addition, the peaks of S1 are shifted toward much higher 2θ values than those of S2, which

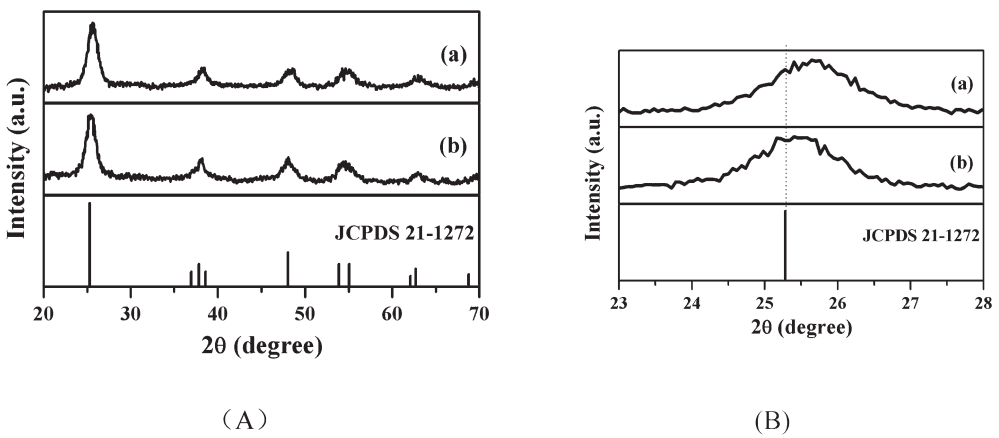

Fig. 1 (A) XRD patterns of S1 (a) and S2 (b). The standard data for anatase phase TiO_2 (JCPDS no. 21-1272) are also presented for comparison. (B) Local amplification of the (101) peaks of S1 (a), S2 (b), and the standard anatase phase TiO_2 (JCPDS no. 21-1272).

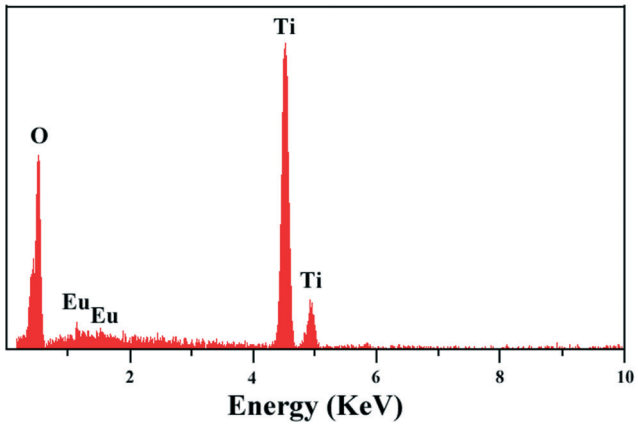

Fig. 2 EDS spectrum of TiO_2:Eu^{3+} solid microspheres (S1).

also indicate that Eu^{3+} ions in S1 are doped much more effectively than Eu^{3+} ions in S2.

In order to investigate the element composition, the as-prepared samples were analysed by energy-dispersive spectrometry (EDS) and the EDS of S1 is shown in Fig. 2 (the EDS of S2 is similar to that of S1 and so it was not shown here). The EDS result confirms the presence of titanium (Ti), oxygen (O), and europium (Eu) elements in TiO_2:Eu^{3+} solid microspheres and core–shell microspheres. No other peaks of impurity elements were detected, which gives further support to the XRD analysis above.

The chemical components of the as-synthesized Eu-doped TiO_2 samples were further analyzed by X-ray photoelectron spectroscopy. Typical XPS survey scans of S1 and S2 (solid and core–shell TiO_2:Eu^{3+}) over a large energy range are presented in Fig. 3A. It can be seen that there are Eu 3d, Eu 4d, Ti 2p,

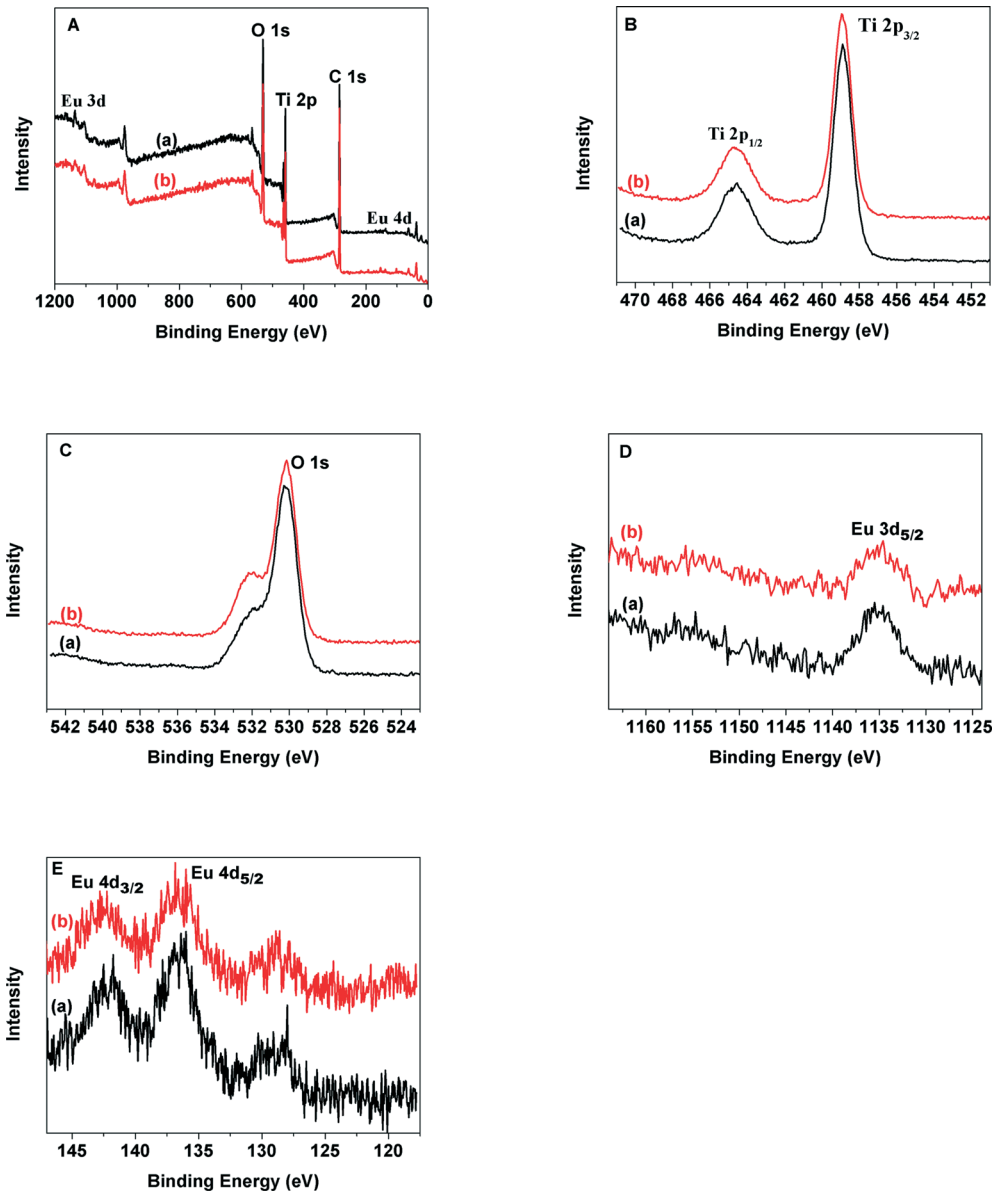

Fig. 3 XPS spectra of the survey (A), Ti 2p (B), O 1s (C), Eu 3d (D), and Eu 4d (E) for solid TiO_2:Eu^{3+} (a) and core–shell TiO_2:Eu^{3+} (b).

O 1s, and C 1s XPS lines; among these, the C 1s spectrum is due to the contamination of CO_2 in air and carbon on the substrate, while the existence of Eu 3d, Eu 4d, Ti 2p, and O 1s further confirms the EDS results. Fig. 3B shows the Ti $2p_{1/2}$ and Ti $2p_{3/2}$ spectra of S1 and S2. The Ti $2p_{3/2}$ peaks of S1 and S2 are all shifted from 459.4 eV in pure TiO_2 (ref. 27) to 458.9 eV in S1 and S2. This shifting represents an intermediate oxidation state of Ti from tetra- to trivalent[27] due to the doping of Eu^{3+}. Fig. 3C shows the O 1s spectra of S1 and S2. As reported in the literature,[28,29] the O 1s binding energy of pure TiO_2 is ~530.0 eV. However, in the O 1s spectra of S1 and S2, an intense peak was found at a BE of 530.2 eV and a shoulder at a BE of 532.0 eV. The Eu $3d_{5/2}$ and Eu $4d_{5/2}$ peaks of S1 are found at 1135.4 eV and 136.7 eV, respectively, while the Eu $3d_{5/2}$ peak and Eu $4d_{5/2}$ peak of S2 are at 1134.7 eV and 137.1 eV, respectively. The data available in the literature for Eu_2O_3 are 1134.2 and 135.0 eV for the Eu $3d_{5/2}$ and Eu $4d_{5/2}$ peaks, respectively.[30,31] These different binding energies correspond to different chemical environments,[32] which further indicate that the crystal environments of Eu^{3+} are different for the solid and the core–shell microspheres, and Eu^{3+} ions have been effectively doped into S1 and S2 rather than simply being mixed.

The morphology and structure of the products were examined using a scanning electron microscope (SEM) and a transmission electron microscope (TEM). Fig. 4a shows a panoramic SEM image of the as-prepared S1. From Fig. 4a, it can be seen that S1 mainly contains uniform spheres with an average diameter of about 2.0 μm. A high-magnification SEM image reveals that the surface of the microspheres is smooth (Fig. 4b). TEM images of S1 (Fig. 4c and d) clearly show that the sample consists of uniform, smooth, monodisperse, and solid microspheres with diameters of about ~2.0 μm. In contrast, S2 is composed of uniform spheres with a mean diameter of ~2.4 μm and there appear two or three microspheres attached together (Fig. 5a). More careful examination of the high-magnification SEM image (Fig. 5b) verifies that the surface of S2 is rough and the core–shell structure can be seen more clearly from the SEM image of the cracked microsphere. As shown in Fig. 5c and d, the dark center and pale edge of the microspheres further prove the core–shell nature of S2. The shell thickness of the spheres is about 50 nm, which is identical to the SEM observations. The results reveal that the amount of ethanol plays a critical role in the formation of TiO_2:Eu^{3+} microspheres.

To examine the role of the amount of ethanol, different amounts of ethanol were used while the other reaction parameters remained unchanged. Fig. 6 shows the SEM images of solvothermal samples obtained when different amounts of ethanol were added. From Fig. 6, it can be seen that the obtained microspheres are solid and their surfaces are smooth when small amounts of ethanol (15 mL, 18 mL, and 21 mL) are added. However, with the increase of the amount of ethanol to 22 mL, the surface of the microspheres tends to become rough. Upon further increasing the amount of ethanol to 24 mL, rough and core–shell structured microspheres are formed. When the amount of ethanol reached 30 mL, obvious core–shell structured and uniform microspheres can be clearly observed. In addition, the core–shell structured microspheres are a little larger than the solid microspheres.

To shed light on the formation of the two kinds of microspheres and to enrich the crystal growth mechanism of TiO_2 microspheres, time-dependent experiments on S1 and S2 were performed while the other reaction parameters remained unchanged. Interestingly, we find that there is a large difference between the two kinds of microspheres. With the

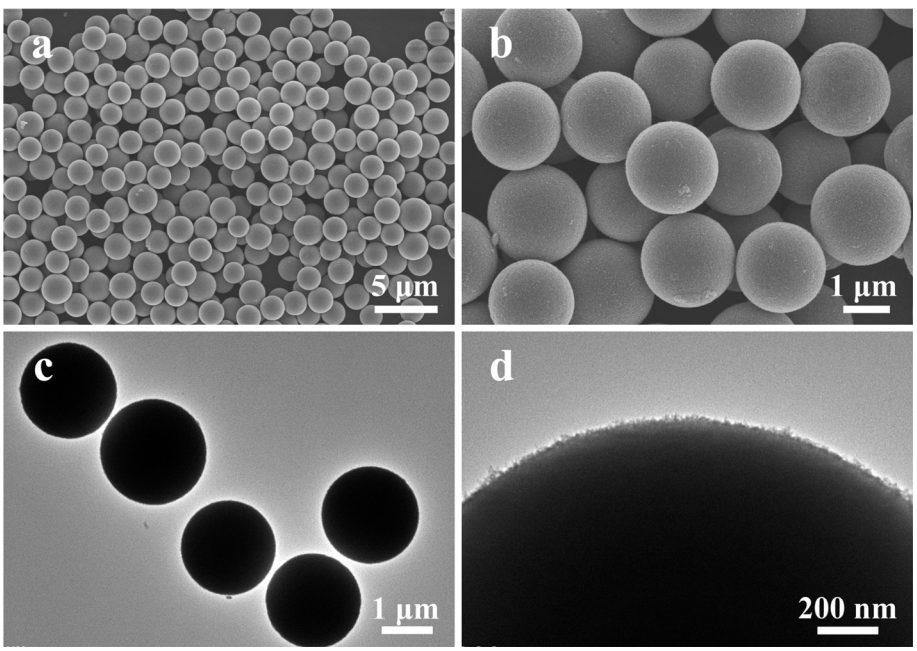

Fig. 4 SEM (a and b) and TEM (c and d) images of the as-prepared sample S1.

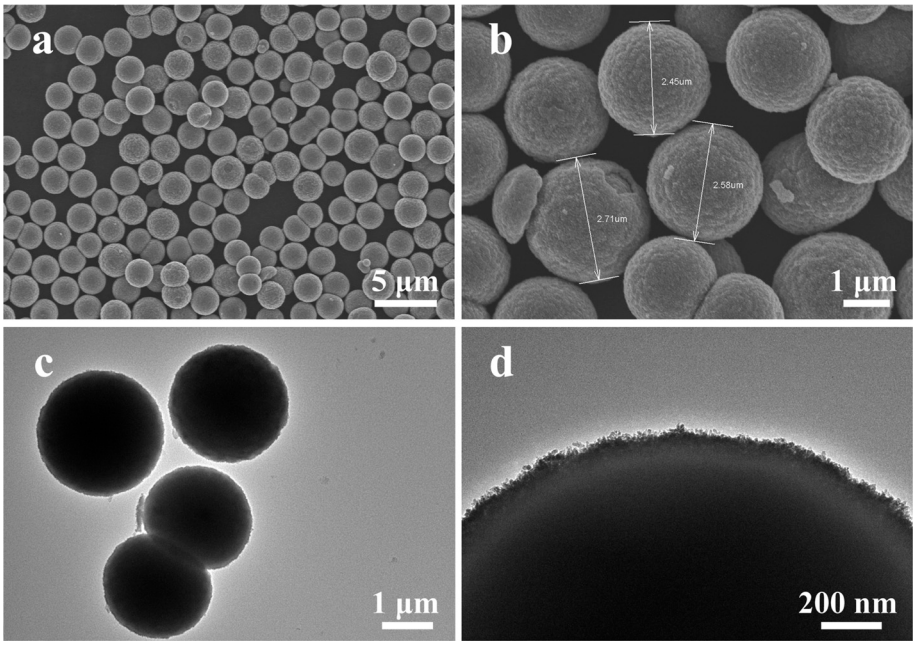

Fig. 5 SEM (a and b) and TEM (c and d) images of the as-prepared sample S2.

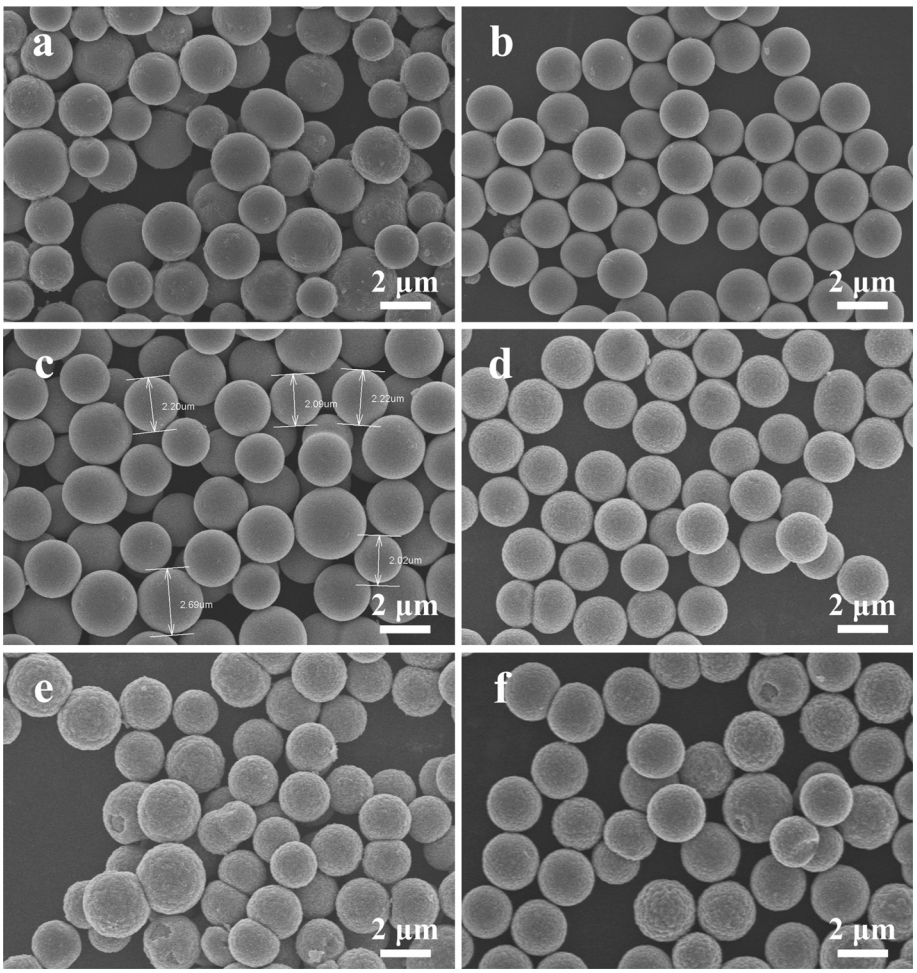

Fig. 6 SEM images of the as-prepared samples with different amounts of ethanol: (a) 15 mL, (b) 18 mL, (c) 21 mL, (d) 22 mL, (e) 24 mL, and (f) 30 mL.

increase of the hydrothermal reaction time, the morphology of the solid microspheres is not changed, that is, they are still solid microspheres. However, the hydrothermal time has a great influence on the core–shell structured microspheres. With a short hydrothermal reaction time (45 min and 90 min, Fig. 7a and b), there is no gap between the core and the shell. When the hydrothermal reaction time increased to 12 h, a small gap appeared. Furthermore, as shown in Fig. 7c–f, the core became smaller while the shell got thicker, that is, the gap became bigger with increasing hydrothermal reaction time (12 h, 18 h, 4 days, and 6 days). On the basis of these images, it is speculated that the core–shell structured microspheres undergo an Ostwald ripening process when the hydrothermal time is prolonged as reported by Yuming Cui.[22] This is a sophisticated process of the Ostwald ripening mechanism; during this process, the inner titania crystallites of the core, which have a higher surface energy and a smaller diameter, would dissolve and transfer to the outer space in the oxide shells and redeposit and recrystallize on the better crystallized TiO_2 nanoparticles of the shell.

Summing up the above results and discussion, the most plausible formation mechanisms of the solid and core–shell structured microspheres are proposed and schematically illustrated in Fig. 8. First, as the literature[22,33,34] reported, the aggregated acid-stabilized $Ti(OBu)_nL_{4-n}$–PEG–urea globules are formed by weak coordination interaction and hydrogen bonding. For the system with a small amount of added solvent ethanol, the concentration of PEG is higher and the PEG chains in the globules are relatively denser than those of the system with a large amount of added ethanol. Second, $Ti(OBu)_4$ is gradually hydrolyzed into TiO_2 under the action of the soft templates $Ti(OBu)_nL_{4-n}$–PEG–urea globules. For the S1 system, the high viscosity and dense chains make the movement of the formed TiO_2 difficult and solid microspheres are gradually formed. However, for the S2 system, increasing the amount of solvent ethanol increases the pressure of the system; the existing pressure and temperature gradients from the outer surface to the inner surface of the $Ti(OBu)_nL_{4-n}$–PEG–urea globules allow the formation of TiO_2 nanoparticle layers on the exterior of the globules. The relatively low viscosity and loose chains allow the formed TiO_2 to move to the exterior of the globules. Just as the literature[22] suggested, the hydrothermal decomposition of the urea molecules results in tiny CO_2 gas bubbles in the globules, and the tiny gas bubbles are confined in the globule by the surface-covered TiO_2 nanoparticles. Therefore, the core–shell

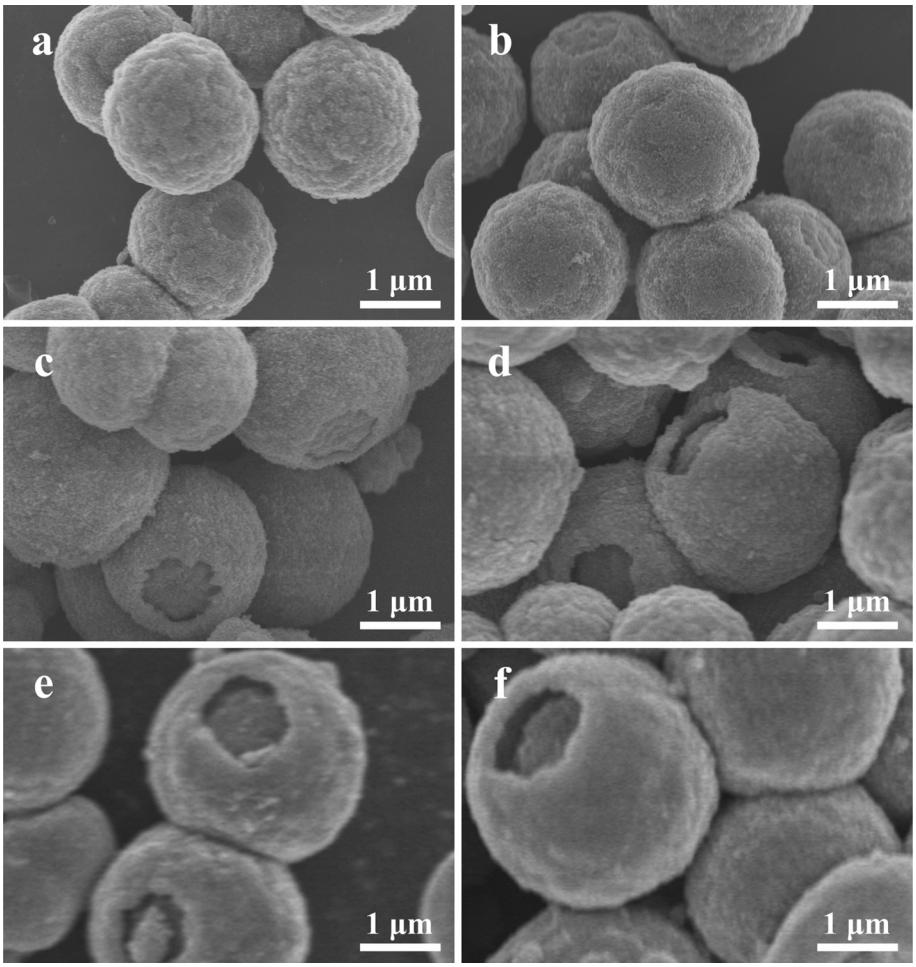

Fig. 7 SEM images of S2 at different hydrothermal reaction times: (a) 45 min, (b) 90 min, (c) 12 h, (d) 18 h, (e) 4 days, and (f) 6 days.

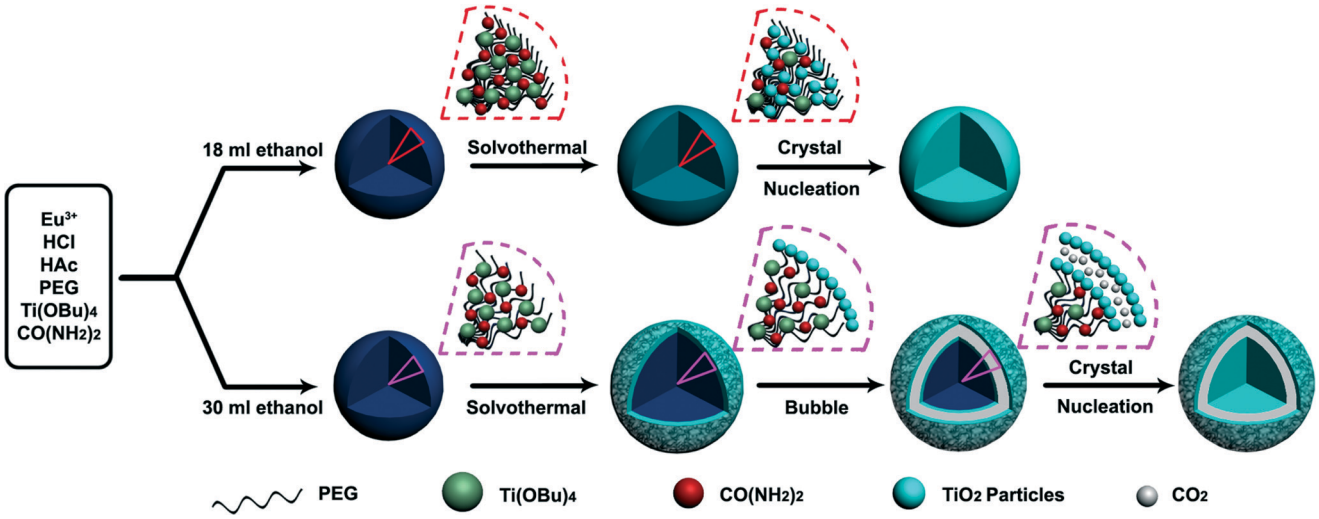

Fig. 8 Schematic illustration of the formation process of TiO_2:Eu^{3+} microspheres.

structured TiO_2 microspheres are formed by the reaction of acid-stabilized $Ti(OBu)_nL_{4-n}$ with $NH_3{\cdot}H_2O$ released from the hydrothermal decomposition of urea in the confined interior of the microspheres during the hydrothermal process.

Fig. 9 shows the emission and excitation (inset) spectra of the obtained S1 and S2, demonstrating that both of them have similar photoluminescence (PL) properties. The excitation spectrum, monitored at 612 nm emission of Eu^{3+} ($^5D_0 \rightarrow {}^7F_2$), consists of the characteristic excitation lines of Eu^{3+} within its $^4f_6$ configuration from 300 to 500 nm. The peaks at 361, 384, 394, 415, and 464 nm can be clearly observed which correspond to the $^7F_0 \rightarrow {}^5D_4$, $^7F_0 \rightarrow {}^5G_2$, $^7F_0 \rightarrow {}^5L_6$, $^7F_0 \rightarrow {}^5D_3$, and $^7F_0 \rightarrow {}^5D_2$ transitions of Eu^{3+}, respectively. Upon excitation at 394 nm, the emission spectra of both the solid and the core–shell TiO_2:2% Eu^{3+} microspheres are composed of a group of lines peaking at about 578, 590, 612, 651, and 696 nm. They are assigned to the $^5D_0 \rightarrow {}^7F_J$ (J = 0, 1, 2, 3, 4) transitions of the Eu^{3+} ions. The $^5D_0 \rightarrow {}^7F_1$ transition at 590 nm is the parity-allowed magnetic dipole transition (ΔJ = 1), and the $^5D_0 \rightarrow {}^7F_2$ transition at 612 nm is the electric dipole transition (ΔJ = 2).[35] It is well known that the relative intensities of the $^5D_0 \rightarrow {}^7F_1$ and $^5D_0 \rightarrow {}^7F_2$ transitions are also determined by the symmetry of the crystal sites of the Eu^{3+} ions. If Eu^{3+} ions occupy a site with inversion symmetry, the $^5D_0 \rightarrow {}^7F_1$ transition dominates while if Eu^{3+} ions occupy a site without inversion symmetry, the $^5D_0 \rightarrow {}^7F_2$ transition predominates.[36] In the cases of S1 and S2, the most prominent emission originates from the $^5D_0 \rightarrow {}^7F_2$ transition; therefore, the Eu^{3+} ions locate at low-symmetry local sites in S1 and S2. Anatase adopts a tetragonal symmetry with the space group $I4_1/amd$, and the site symmetries for the Ti^{4+} ions are D_{2d} in anatase. According to the branching rules of the 32 point groups, the substitution of the larger Eu^{3+} ions for Ti^{4+} ions creates oxygen vacancies and lattice distortions in the TiO_2 host and changes the site symmetry of the Eu^{3+} ions from the exact D_{2d} symmetry to lower site symmetry. Eu^{3+} symmetry could be defined by the asymmetric ratio (A_{21}) of the integrated intensities of $^5D_0 \rightarrow {}^7F_2$ to $^5D_0 \rightarrow {}^7F_1$. A_{21} is calculated to be 3.27 for S1 and 3.23 for S2; this difference is attributed to the fact that Eu^{3+} ions in S1 are doped much more effectively than Eu^{3+} ions in S2 (as XRD results have proved).

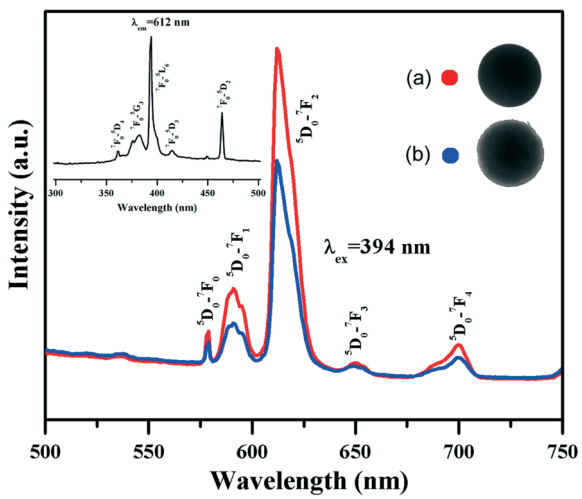

Fig. 9 PL emission spectra of the (a) solid and (b) core–shell structured TiO_2:Eu^{3+} microspheres and the typical excitation spectrum (inset).

Herein, it should be noted that the morphologies of the obtained samples have an important effect on their luminescence intensity, provided that the two samples have the same concentration of europium ions. As presented in Fig. 9, the PL intensity of the solid microspheres is higher than that of the core–shell ones, which might be due to the fewer defects and much more effective doping of Eu^{3+} ions into the solid microspheres. It is well known that defects of phosphor crystals provide non-radiative recombination routes for electrons and holes and lead to luminescence quenching.[37,38] It can be speculated that the surface areas of the rough core–shell microspheres are higher than those of the solid

microspheres. A large surface area usually introduces a large number of defects into the phosphor crystal.[39] As a result, the PL intensity of the solid microspheres is higher than that of the core–shell microspheres. On the other hand, the Eu^{3+} ions in S1 are doped much more effectively than the Eu^{3+} ions in S2, which also results in the higher PL intensity of the solid microspheres compared to that of the core–shell ones.

4. Conclusions

In summary, anatase TiO_2:Eu^{3+} microspheres have been successfully prepared by a facile one-step hydrothermal synthesis method. The microspheres can be easily tuned from solid to core–shell structure by the amount of solvent ethanol. Furthermore, the shell and core sizes of the core–shell microspheres can be controlled by the hydrothermal time through the Ostwald ripening process. The possible formation mechanisms are proposed. In addition, it is also observed that the PL intensity of Eu^{3+} ions depends on the structure of the microspheres. Our work presents a new idea for designing and synthesizing inorganic functional materials.

Acknowledgements

This work is financially supported by the National Natural Science Foundation of China (grant no. 21171066 and 51272085), the Opening Research Funds Projects of the State Key Laboratory of Inorganic Synthesis and Preparative Chemistry, College of Chemistry, Jilin University (2013-27), and the Key Technology and Equipment of Efficient Utilization of Oil Shale Resources (no. OSR-05).

References

1 Y. Deng, D. Qi, C. Deng, X. Zhang and D. Zhao, *J. Am. Chem. Soc.*, 2008, **130**, 28–29.
2 Q. Peng, Y. J. Dong and Y. D. Li, *Angew. Chem., Int. Ed.*, 2003, **42**, 3027–3030.
3 V. R. Sinha, A. K. Singla, S. Wadhawan, R. Kaushik, R. Kumria, K. Bansal and S. Dhawan, *Int. J. Pharm.*, 2004, **274**, 1–33.
4 Z. W. Zhang, L. Y. Cao, J. F. Huang, D. Q. Wang, J. P. Wu and Y. J. Cai, *Ceram. Int.*, 2013, **39**, 2695–2698.
5 S. Dehghanpour, A. Mahmoudi, M. Mirsaeed-Ghazi, N. Bazvand, S. Shadpour and A. Nemati, *Powder Technol.*, 2013, **246**, 148–156.
6 R. Razali, A. K. Zak, W. H. Abd Majid and M. Darroudi, *Ceram. Int.*, 2011, **37**, 3657–3663.
7 Z. Q. Sun, J. H. Kim, Y. Zhao, F. Bijarbooneh, V. Malgras, Y. Lee, Y. M. Kang and S. X. Dou, *J. Am. Chem. Soc.*, 2011, **133**, 19314–19317.
8 A. R. Tao, S. Habas and P. D. Yang, *Small*, 2008, **4**, 310–325.
9 T. K. Sau and A. L. Rogach, *Adv. Mater.*, 2010, **22**, 1781–1804.
10 J. B. Yin, L. Q. Xiang and X. P. Zhao, *Appl. Phys. Lett.*, 2007, **90**(1–3), 113112.
11 W. Q. Luo, R. F. Li, G. K. Liu, M. R. Antonio and X. Y. Chen, *J. Phys. Chem. C*, 2008, **112**, 10370–10377.
12 S. Sandoval, J. Yang, J. G. Alfaro, A. Liberman, M. Makale, C. E. Chiang, I. K. Schuller, A. C. Kummel and W. C. Trogler, *Chem. Mater.*, 2012, **24**, 4222–4230.
13 H. Hafez, J. Wu, Z. Lan, Q. Li, G. Xie, J. Lin, M. Huang, Y. Huang and M. Abdel-Mottaleb, *Nanotechnology*, 2010, **21**, 415201.
14 P. Haro-González, M. Pedroni, F. Piccinelli, L. Martín, S. Polizzi, M. Giarola, G. Mariotto, A. Speghini, M. Bettinelli and I. Martín, *J. Lumin.*, 2011, **131**, 2473–2477.
15 J. Yin and X. Zhao, *Mater. Chem. Phys.*, 2009, **114**, 561–568.
16 D. K. Yi and D.-Y. Kim, *Nano Lett.*, 2003, **3**, 207–211.
17 F. Wang, J. Jiu, L. Pei, K. Nakagawa, S. Isoda and M. Adachi, *Mater. Lett.*, 2007, **61**, 488–490.
18 L. Li, C. K. Tsung, Z. Yang, G. D. Stucky, L. D. Sun, J. F. Wang and C. H. Yan, *Adv. Mater.*, 2008, **20**, 903–908.
19 Y. Tian, J. Zhang, J. C. Ma and X. Jia, *J. Colloid Interface Sci.*, 2012, **385**, 1–7.
20 J. Feng, Y. Hong, J. Zhang, P. Wang, Z. Hu, Q. Wang, L. Han and Y. Zhu, *J. Mater. Chem. A*, 2014, **2**, 1502–1508.
21 G. An, C. Yang, S. Jin, G. Chen and X. Zhao, *J. Mater. Sci.*, 2013, **48**, 5483–5488.
22 Y. Cui, L. Liu, B. Li, X. Zhou and N. Xu, *J. Phys. Chem. C*, 2010, **114**, 2434–2439.
23 H. G. Yang and H. C. Zeng, *J. Phys. Chem. B*, 2004, **108**, 3492–3495.
24 H. Li, Z. Bian, J. Zhu, D. Zhang, G. Li, Y. Huo, H. Li and Y. Lu, *J. Am. Chem. Soc.*, 2007, **129**, 8406–8407.
25 H. Li, Y. Sheng, H. Zhang, J. Xue, K. Zheng, Q. Huo and H. Zou, *Powder Technol.*, 2011, **212**, 372–377.
26 D. Q. Chen and Y. S. Wang, *Nanoscale*, 2013, **5**, 4621–4637.
27 S. Watanabe, X. L. Ma and C. S. Song, *J. Phys. Chem. C*, 2009, **113**, 14249–14257.
28 S. P. Chenakin, G. Melaet, R. Szukiewicz and N. Kruse, *J. Catal.*, 2014, **312**, 1–11.
29 N. Kruse and S. Chenakin, *Appl. Catal., A*, 2011, **391**, 367–376.
30 F. Mercier, C. Alliot, L. Bion, N. Thromat and P. Toulhoat, *J. Electron Spectrosc. Relat. Phenom.*, 2006, **150**, 21–26.
31 W.-D. Schneider, C. Laubschat, I. Nowik and G. Kaindl, *Phys. Rev. B: Condens. Matter Mater. Phys.*, 1981, **24**, 5422–5425.
32 X. L. Tan, Q. H. Fan, X. K. Wang and B. Grambow, *Environ. Sci. Technol.*, 2009, **43**, 3115–3121.
33 X. Zhou, S. Chen, D. Zhang, X. Guo, W. Ding and Y. Chen, *Langmuir*, 2006, **22**, 1383–1387.
34 X. Zhou, D. Zhang, Y. Zhu, Y. Shen, X. Guo, W. Ding and Y. Chen, *J. Phys. Chem. B*, 2006, **110**, 25734–25739.
35 Y. Y. Hui and C. F. Lin, *Mater. Lett.*, 2007, **61**, 3802–3804.
36 Y. H. Zheng, H. P. You, G. Jia, K. Liu, Y. H. Song, M. Yang and H. J. Zhang, *Cryst. Growth Des.*, 2009, **9**, 5101–5107.
37 Q. Zhao, N. Guo, Y. C. Jia, W. Z. Lv, B. Q. Shao, M. M. Jiao and H. P. You, *J. Colloid Interface Sci.*, 2013, **394**, 216–222.
38 B. L. Abrams and P. H. Holloway, *Chem. Rev.*, 2004, **104**, 5783–5801.
39 Q. Zhao, Y. Zheng, N. Guo, Y. Jia, H. Qiao, W. Lv and H. You, *CrystEngComm*, 2012, **14**, 6659–6664.